Title

Determination of rotatable and frozen CoO spins and their relationship to exchange bias in CoO/Fe/Ag(001)

Authors

Wu, J.
Park, J.
Kim, W.
et al.

Publication Date

2010-06-30

Determination of rotatable and frozen CoO spins and their relationship to exchange bias in CoO/Fe/Ag(001)

J. Wu[1], J. S. Park,[1] W. Kim[1, 2], E. Arenholz,[3] M. Liberati,[3] A. Scholl,[3] Y. Z. Wu,[4] Chanyong Hwang[2], and Z. Q. Qiu[1]

[1] Department of Physics, University of California at Berkeley, Berkeley, California 94720, USA

[2] Korea Research Institute of Standards and Science,Yuseong, Daejeon 305-340, Koera

[3] Advanced Light Source, Lawrence Berkeley National Laboratory, Berkeley, California 94720, USA

[4] Dept. of Physics, Fudan University, Shanghai, P. R. China

Abstract

The exchange bias of epitaxially grown CoO/Fe/Ag(001) was investigated using X-ray Magnetic Circular Dichroism (XMCD) and X-ray Magnetic Linear Dichroism (XMLD) techniques. A direct XMLD measurement on the CoO layer during the Fe magnetization reversal shows that the CoO compensated spins are rotatable at thinner thickness and frozen, i.e. fixed in direction to the lattice, at larger thickness. By a quantitative determination of the rotatable and frozen CoO spins as a function of the CoO film thickness, we find the remarkable result that the exchange bias is well established before frozen spins are detectable in the CoO film, contrary to the common assumption that the majority of antiferromagnetic spins need to be frozen to generate the exchange bias. We further show that the rotatable/frozen CoO spins are uniformly distributed in the CoO film.

PACS numbers: 75.70.Ak

As a ferromagnetic(FM)/antiferromagnetic(AFM) system is cooled down within a magnetic field to below the Néel temperature (T_N) of the AFM material, the shift of the FM hysteresis loop in the applied magnetic field is referred to as exchange bias [1]. Investigation of exchange bias has been one of the most active areas in nanomagnetism research because of its importance to spintronics technology, especially to the design of spin valves [2]. While it is well accepted that AFM order in a FM/AFM system is responsible for the exchange bias [3,4], it remains unclear on how the AFM spins behave during the FM magnetization reversal. Consequently, different AFM spin structures have been proposed to explain the exchange bias [5,6,7,8]. Most measurements are based on the FM layer hysteresis loops which explore only indirectly the AFM spin behavior during the FM magnetization reversal, such as in the study of training effect [9,10,11], pinning orientation effect [12,13,14,15], and finite size effect [16,17], etc. Recently, the development of X-ray Magnetic Circular Dichroism (XMCD) and X-ray Magnetic Linear Dichroism (XMLD) [18] allows an element-specific study of the FM/AFM systems. The result shows clearly the correlation between the FM and the AFM domains, and the existence of a small amount of ~~induced~~ uncompensated spins in the AFM layer [19]. These uncompensated spins in the AFM layer were consequently used to probe the AFM spin behaviors by measuring the magnetization reversal of these uncompensated spins. The result shows that only a small percentage of the uncompensated spins is pinned to account for the exchange bias [20,21,22,23]. Moreover, the pinned uncompensated AFM spins actually extend into the AFM layer [24], suggesting a bulk-like effect of the AFM spins in generating the exchange bias. In fact, an alternative approach by doping the AFM layer with non-magnetic elements [25,26,27,28,] and by studying a FM/AFM/FM trilayer also show that the spins in the entire AFM layer are relevant to the exchange bias [29]. Despite the above summarized progress, the compensated AFM spin behavior remains unclear during the FM layer reversal in exchange bias systems. It is usually assumed that the AFM spins in a FM/AFM system should be frozen, i.e. their orientation fixed to the lattice to generate an exchange bias. However, one direct measurement on Co/bulk NiO(001) shows that the NiO spins at the Co/NiO interface may exhibit a spring-like winding structure during the Co magnetization alignment [30]. This result is for bulk NiO substrate where the majority bulk NiO spins away from the interface are frozen and cannot be applied to AFM thin films. It raises a critical issue, i.e. whether it is necessary to freeze the majority of the AFM compensated spins to generate an exchange bias.

Unfortunately, this question has never been addressed directly in an experiment for FM/AFM thin film systems. A clarification of this issue obviously requires a direct measurement of the AFM compensated spins during the FM magnetization reversal. XMLD is currently the only available technique to make such a measurement. However, unlike XMCD, which has a high sensitivity and can be applied to almost any types of FM thin films, XMLD has a weaker signal and can be applied only to a few types of single crystalline AFM films. That is probably why only Co/bulk NiO(001) has been measured so far on the response of the AFM NiO spins to an applied magnetic field. In this Letter, we report an experimental study of CoO/Fe/Ag(001) single crystalline thin films. Using XMLD measurements within a magnetic field parallel and perpendicular to the field cooling direction, we are able to separate for the first time the rotatable and frozen compensated CoO spins during the Fe magnetization reversal. We find the remarkable result that as the CoO thickness increases, the exchange bias is well established before the frozen spins are detected in CoO film. Using a 2ML NiO as a probe layer, we further show that the rotatable and frozen CoO spins are uniformly distributed in the CoO film, suggesting that the exchange bias is determined by the bulk spin structure of the CoO film.

A Ag(001) single crystal substrate was prepared in an ultra-high vacuum system by cycles of Ar ion sputtering at ~2keV and annealing at 600^{o}C. A 15 monolayer (ML) Fe film was grown on top of the Ag(001) substrate. Then a CoO wedge (0-4nm) was on top of the Fe film by a reactive deposition of Co under an oxygen pressure of 1×10^{-6} Torr. Low Energy Electron Diffraction (LEED) shows well-defined diffraction spots, indicating the formation of epitaxial single crystalline CoO film which agrees with the literature result [31]. The sample is covered by a 2nm Ag protection layer and then measured at beamlines 4.0.2 and 11.0.1 of the Advanced Light Source (ALS) of the Lawrence Berkeley National Laboratory. As reported in the literature, Fe film on Ag(001) has a bcc structure with the Fe [001] axis parallel to the Ag [110] axis and CoO film on Fe(001) has an fcc structure with the CoO [110] axis parallel to the Fe [100] axis.

The CoO/Fe/Ag(001) sample were measured using photoemission electron microscopy (PEEM) for domain imaging and employing magnetic spectroscopy and magnetic hysteresis loops. XMLD effect is clearly seen by measuring the X-ray absorption spectrum (XAS) at the CoO L_3 edge (Fig. 1) with different X-ray polarization directions. The L_3 ratio (R_{L3}), defined by the ratio of the XAS intensity at 778.1 eV and 778.9 eV, is used to quantify the XMLD effect [32]. We first present element-specific

domain imaging result on the as-grown sample of CoO(6 nm)/Fe(15 ML)/Ag(001) after cooling the sample to 90 K. We find that the CoO domains follow exactly the Fe domains (Fig. 1b), showing that the Fe magnetization aligns the AFM CoO spin axis. Noting that Fe [100] axis is parallel to CoO [110] axis, the L3 ratio analysis [32,33,34] then leads to the conclusion that the in-plane CoO AFM spins have a 90^{o}-coupling to the Fe spins in the CoO(6 nm)/Fe(15ML)/Ag(001) sample.

For the spectroscopy experiments/measurements the sample was cooled down to 90 K within a 4 kOe magnetic field along the Fe [100] crystal axis. From the PEEM result, the Fe magnetization in the [100] axis results in a CoO spin direction in the Fe [0±10] direction after cooling the sample below the Néel temperature. Element-specific Fe and CoO hysteresis loops are measured at 90 K with the applied field in the field cooling direction. A small transverse in-plane field was applied during the hysteresis loop measurement to ensure a rotational Fe magnetization reversal. In the XMLD measurement of the CoO L3 edge, the x-ray polarization direction is also parallel to the field cooling direction. Fig. 2 depicts representative hysteresis loops of CoO/Fe(15ML)/Ag(001) at two different CoO thicknesses. While the Fe film exhibits expected square shape hysteresis loop, the most interesting observation is the appearance of the CoO XMLD hysteresis loop (Fig. 2) in d_{CoO}=2 nm sample. No XMCD is observed at the Co L3,2 edges. Consequently, the Co XMLD measures the CoO compensated spins. The presence of the CoO hysteresis loop shows clearly that the CoO compensated spins also rotate during the Fe magnetization reversal. In contrast, the absence of the CoO hysteresis loop in d_{CoO}=5 nm sample shows that the CoO spins are totally frozen in this case during the Fe magnetization reversal. The CoO XMLD confirms the antiferromagnetic order fo the film. It is worth pointing out that our result is different from the Co/bulk NiO(001) result which shows a non zero response of the NiO spins in the surface near region to the external magnetic field [30]. We attribute this difference to the different NiO and CoO magnetic properties, i.e. the fact that CoO exhibits a much stronger magnetic anisotropy than NiO. The CoO hysteresis loop of the d_{CoO}=2 nm sample exhibits two peaks at the positive/negative coercive fields of the Fe hysteresis loops. This result shows that the CoO AFM spins rotate together with the Fe magnetization in an external magnetic field: as the Fe magnetization is saturated in the positive and negative field directions, the CoO spins have the same spin axis to give the same XMLD value; as the Fe magnetization rotates by 90^{o} at the Fe coercive field, the CoO spins also rotate by

90^o to give a maximum (peak) XMLD value. Then the result of Fig. 2 shows that the AFM CoO spins are rotatable at thinner thickness and frozen at thicker thickness. This trend should produce a thickness dependent Fe hysteresis loops as a function of the CoO thickness.

Fig. 4 shows the Fe film coercivity (H_C) and exchange bias (H_E) as a function of the CoO thickness. As expected, the H_C and H_E increases with CoO thickness and saturate at thicker CoO thickness. However, while the H_C starts to increase at d_{CoO}~0.2 nm, the H_E develops only above a critical thickness of d_{CoO}=0.8 nm. The increase of the H_C is due to the establishment of the AFM order of the CoO layer [2] and indeed we observe non-zero XMLD signal above d_{CoO}=0.2 nm. Then the onset of H_E at d_{CoO}=0.8 nm shows that the exchange bias does not develop right after the CoO establishes its AFM order at thinner thickness but develops only above a larger CoO thickness. Recognizing the rotatable and frozen behaviors of the CoO spins at thinner and thicker CoO thicknesses (Fig. 2), it is tempting to associate the onset of the exchange bias to the onset of the frozen spins in the CoO layer. There has been no direct measurement in the literature to quantitatively single out the amount of frozen spins in the AFM layer. We carried out the following measurement to separate the rotatable and frozen spins in the CoO layer. We performed XMLD measurement as a function of the polarization angle (ϕ) to obtain the ϕ-dependence of the L3 ratio R_{L3}. The R_{L3} anglar dependence for fixed orientation of the x ray beam to the sample can be approximated has a $\cos^2\phi$ dependence on the polarization angle, i.e., $R_{L3}=A\cos^2\phi+B$, with the coefficient A proportional to the amount of the AFM compensated spins. Therefore a R_{L3}-ϕ measurement would allow the determination of A thus the amount of AFM spins under specific conditions.

We first measured the R_{L3}-ϕ dependence right after the field cooling. Under this condition, both rotatable and frozen CoO spins should be aligned to the same direction so that the R_{L3} difference at $\phi=90^o$ and $\phi=0^o$ [e.g., $\Delta R_{L3}=R_{L3}(90^o)-R_{L3}(0^o)$] is proportional to the total CoO spins. The result (top row of Fig. 3) shows that R_{L3} indeed follows a $\cos^2\phi$ dependence on the polarization angle. We then applied an in-plane magnetic field perpendicular to the field-cooling direction to rotate the Fe magnetization by 90^o in the film plane. Under this condition, the rotatable CoO spins should follow the Fe magnetization to also rotate by 90^o while the frozen CoO spins should remain in their original direction. Then the R_{L3} difference at $\phi=90^o$ and $\phi=0^o$ is proportional to the difference between the frozen and rotatable CoO spins. The result (lower row of Fig. 3) indeed shows a thickness

dependent $\Delta R_{L3}=R_{L3}(90^o)-R_{L3}(0^o)$. At d_{CoO}=6.0 nm, the R_{L3}-ϕ dependence is exactly the same as that for applied field in the field cooling direction (top row of Fig. 3), showing that there is no rotatable spins at this thickness. As the CoO thickness decreases to d_{CoO}=2.5 nm, the R_{L3} difference decreases, showing that some CoO spins rotate away from the field cooling direction in the CoO film. Thinner than d_{CoO}=2.5nm, the R_{L3} difference reverses its sign, showing that there are more rotatable spins than frozen spins in the CoO film. It should be mentioned that R_{L3} always reaches its maximum/minimum value at $\phi=0^o$ or $\phi=90^o$. This behavior rules out the spring-like (or domain wall like) spin structure normal to the CoO film because a spring-like spin structure should lead to a maximum/minimum value of the L3 ratio at an angle between $\phi=0^o$ and $\phi=90^o$ (in an extreme case of a perfect 90^o domain wall structure, the L3 ratio should reach its maximum/minimum value at $\phi=45^o$). The R_{L3} difference for field parallel and perpendicular to the field cooling direction allows us to determine quantitatively the percentage of the frozen spins in the CoO film. Fig. 4 shows the result of the frozen CoO spins as a function of CoO film thickness. The CoO film has no detectable frozen spins below 2.2 nm (with an error bar of ~0.1 nm), becomes partially frozen for 2.2 nm<d_{CoO}<4.5 nm, and has all spins frozen for d_{CoO}>4.5 nm.

We then find the remarkable result that the exchange bias develops even when no frozen CoO spins are detected at d_{CoO}<2.2 nm, reaches ~2/3 of its saturation value at the onset of the frozen spins at d_{CoO}=2.2 nm, and becomes saturated at d_{CoO}=3 nm where 80% of the CoO spins are frozen. This result is contrary to the general concept that majority of AFM spins should be frozen to generate an exchange bias in a FM/AFM system. We estimate an upper limit of no more than ~5% (~0.1nm) of frozen spins below d_{CoO}=2.2 nm. Therefore we conclude that ~5% frozen CoO spins should be enough to generate an exchange bias in CoO/Fe/Ag(001) system. This result may explain why only a small percentage of pinned uncompensated spins would be enough to account for the exchange bias [20-24].

The next question is where the rotatable and frozen CoO spins are located? Are the rotatable spins located near the CoO/Fe interface or throughout the CoO film? To answer this question, we inserted a 2ML NiO probe layer at the CoO/Fe interface and at the surface of CoO/Fe by growing two samples of CoO(wedge)/NiO(2ML)/Fe(15ML)/Ag(001) and NiO(2ML)/CoO(wedge)/Fe(15ML)Ag(001). NiO and CoO have similar lattice constants and grow epitaxially on top of each other so that element-specific XMLD

measurement of the NiO can probe the AFM CoO spin structure at the interface and surface. The result shows that the NiO XMLD signal as a function of the CoO thickness follows exactly the CoO thickness dependence, no matter the NiO is at the CoO/Fe interface or at the Co/Fe surface (Fig. 5). This result shows that the rotatable and frozen spins distribute uniformly inside the entire CoO film, supporting the doping and FM/AFM/FM results [25-29] that the exchange bias depends on the bulk AFM spin structure rather than the AFM spins at the FM/AFM interface only.

In summary, we investigated epitaxially grown CoO/Fe/Ag(001). Using element-specific XMLD measurement, we separate rotatable and frozen spins in antiferromagnetic CoO film. We find that the CoO spins are rotatable below 2.2 nm CoO thickness, become partially frozen between 2.2 nm and 4.5 nm, and saturate above 4.5 nm. Contrary to the expectation, the exchange bias of the Fe film develops d_{Co}>2.2 nm even when no frozen spins are detectable in CoO film, reaches ~2/3 of its saturation value at the onset of frozen CoO spins at d_{Co}=2.2 nm, and saturates at d_{CoO}=3 nm where 80% of the CoO spins are frozen. With the XMLD sensitivity estimation, we conclude that ~5% of frozen CoO spins is enough to establish the exchange bias in CoO/Fe/Ag(001) system. We further show that the rotatable/frozen spins distribute uniformly in the CoO film.

Acknowledgement

This work was supported by National Science Foundation DMR-0803305, U.S. Department of Energy DE-AC02-05CH11231, KICOS through Global Research Laboratory project, and Chinese Education Department.

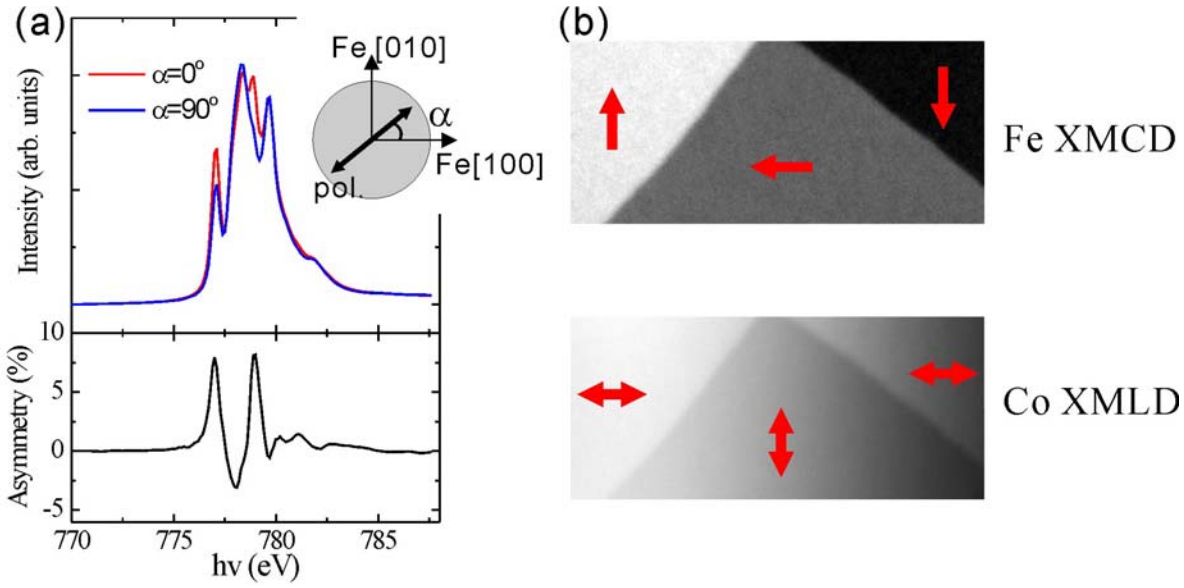

Fig. 1: (a) X-ray Absorption Spectra (XAS) of Co L3 edge taken at two orthogonal linear polarizations ($\phi=0^o$ and 90^o) for CoO(6 nm)/Fe(15 ML)/Ag(001). The asymmetry of two spectra represents XMLD signal. (b) Magnetic domain images of ferromagnetic Fe and antiferromagnetic CoO taken by XMCD and XMLD, respectively. Arrows indicate the orientation of Fe and CoO spins. It is clear that the antiferromagnetic CoO spins are 90^o coupled to Fe spins.

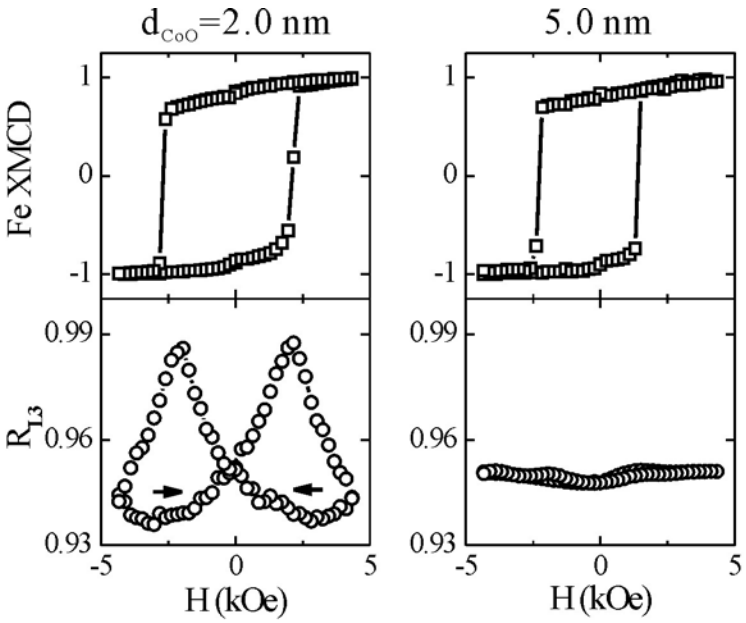

Fig. 2: Hysteresis loops of ferromagnetic Fe and antiferromagnetic CoO for CoO/Fe(15ML)/Ag(001) taken by XMCD and XMLD, respectively. The XMLD hystersis loops of antiferromagntic CoO spins in CoO/Fe(15 ML) bilayer are shown together with corresponding Fe XMCD hystersis loops for two representive CoO thicknesses (2.0 nm and 5.0 nm). Arrows indicate the ramping direction of magnetic field. The presence and absence of the CoO response to the magnetic field at d_{CoO}=2.0 nm and at d_{CoO}=5.0 nm show rotatable and frozen compensated spins in the 2.0 nm and 5.0 nm thick CoO films.

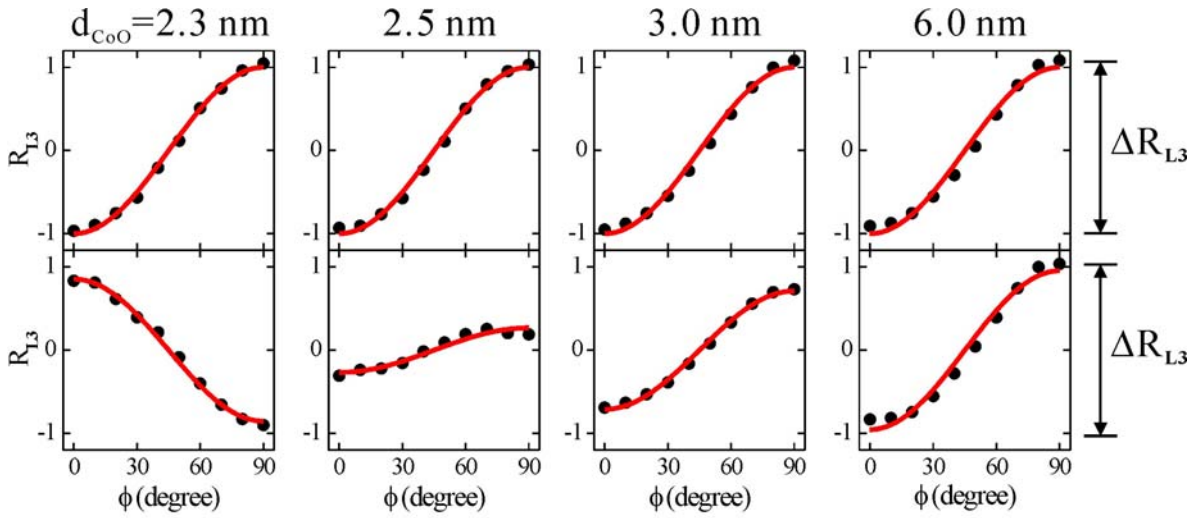

Fig. 3: Polarization angle dependence of the Co L3 ratio measured with a 0.4 Tesla in-plane magnetic field at different CoO thicknesses in CoO/Fe(15ML)/Ag(001). Solid lines are fitting result of $\cos^2\phi$-dependence. The difference of the L3 ratio at $\phi=90^o$ and $\phi=0^o$ is proportional to the sum and subtraction of the frozen and rotatable CoO spins for field parallel (top row) and perpendicular (lower row) to the field cooling direction, respectively.

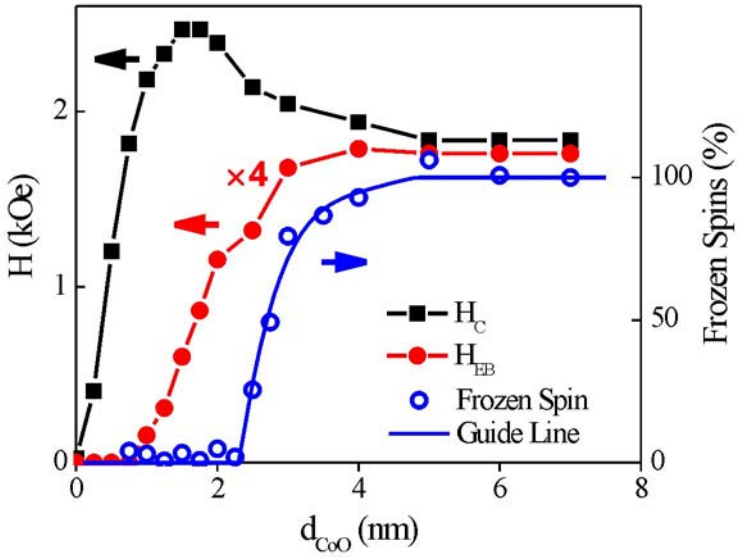

Fig. 4: Fe film coecivity (H_C) and exchange bias (H_E) and the percentage of CoO frozen spins in CoO/Fe(15ML)/Ag(001) as a function of CoO thickness. The remarkable fact is that H_E develops below 2.2 nm CoO thickness where no frozen CoO spins are detected.

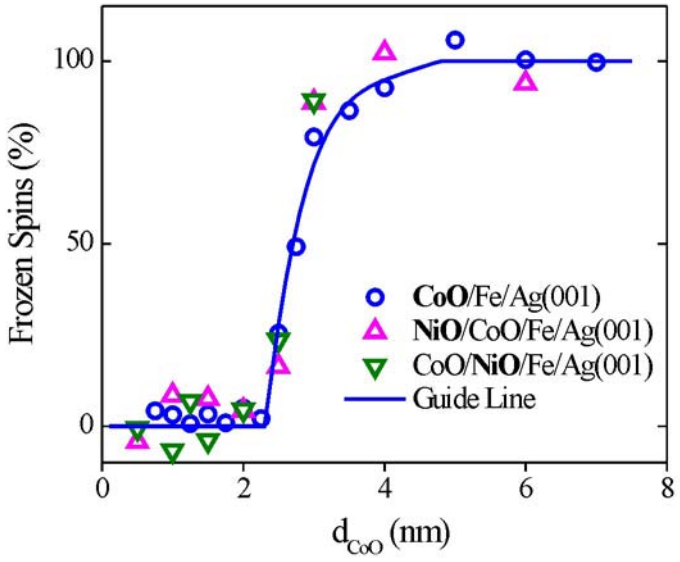

Fig. 5: A 2ML NiO layer is inserted at the top or bottom of CoO to detect the depth-dependent distribution of the frozen CoO spins. The same thickness dependence of the frozen CoO and NiO spins indicate a uniform distribution of the frozen spins in the CoO film.

References:

1. W. H. Meiklejohn and C. P. Bean, Phys. Rev. **102**, 1413 (1956).
2. J. Nogues and I. K. Schuller, J. Magn. Magn. Mater. **192**, 203 (1999).
3. M. G. Blamire, M. Ali, C.-W. Leung, C. H. Marrows, and B. J. Hickey, Phys. Rev. Lett. **98**, 217202 (2007).
4. E. Shipton, K. Chan, T. Hauet T, O. Hellwig, and E. E. Fullerton, Appl. Phys. Lett. **13**, 132509 (2009).
5. N. Koon, Phys. Rev. Lett. **78**, 4865 (1997).
6. T. C. Schulthess and W. H. Butler, Phys. Rev. Lett. **81**, 4516 (1998).
7. D. Mauri, H. C. Siegmann, P. S. Bagus, and E. Kay, J. Appl. Phys. **62**, 3047 (1987).
8. A. P. Malozemoff, Phys. Rev. B **35**, 3679 (1987).
9. T. Hauet, J. A. Borchers, Ph. Mangin, Y. Henry, and S. Mangin, Phys. Rev. Lett. **96**, 067207 (2006).
10. Steven Brems, Kristiaan Temst, and Chris Van Haesendonck, Phys. Rev. Lett. **99**, 067201 (2007).
11. S. K. Mishra, F. Radu, H. A. Dürr, and W. Eberhardt, Phys. Rev. Lett. **102**, 177208 (2009).
12. S. Maat, K. Takano, S. S. Parkin, and Eric E. Fullerton, Phys. Rev. Lett. **87**, 087202 (2001).
13. J. Olamit, Z. P. Li, I. K. Schuller, and K. Liu, Phys. Rev. B **73**, 024413 (2006).
14. H. Ouyang, K.-W. Lin, C.-C. Liu, Shen-Chuan Lo, Y.-M. Tzeng, Z.-Y. Guo, and J. van Lierop, Phys. Rev. Lett. **98**, 097204 (2007)
15. X. P. Qiu, D. Z. Yang, S. M. Zhou, R. Chantrell, K. O'Grady, U. Nowak, J. Du, X. J. Bai, and L. Sun, Phys. Rev. Lett. **101**, 147207 (2008).
16. K. Liu, S.M. Baker, M. Tuominen, T. P. Russell, I. K. Schuller, Phys. Rev. B **63**, 060403 (2001).
17. J. Sort, A. Hoffmann, S.-H. Chung, K. S. Buchanan, M. Grimsditch, M. D. Baró, B. Dieny, and J. Nogués, Phys. Rev. Lett. **95**, 067201 (2005).
18. J. Stöhr, A. Scholl, T. J. Regan, S. Anders, J. Lüning, M. R. Scheinfein, H. A. Padmore, and R. L. White, Phys. Rev. Lett. **83**, 1862 (1999).
19. H. Ohldag, T. J. Regan, J. Stöhr, A. Scholl, F. Nolting, J. Lüning, C. Stamm, S. Anders, and R. L. White, Phys. Rev. Lett. **87**, 247201 (2001).
20. H. Ohldag, A. Scholl, F. Nolting, E. Arenholz, S. Maat, A. T. Young, M. Carey, and J. Stöhr, Phys. Rev. Lett. **91**, 017203 (2003).

21. S. Roy, M. R. Fitzsimmons, S. Park, M. Dorn, O. Petracic, Igor V. Roshchin, Zhi-Pan Li, X. Batlle, R. Morales, A. Misra, X. Zhang, K. Chesnel, J. B. Kortright, S. K. Sinha, and Ivan K. Schuller, Phys. Rev. Lett. 95, 047201 (2005).

22. Hendrik Ohldag, Hongtao Shi, Elke Arenholz, Joachim Stöhr, and David Lederman, Phys. Rev. Lett. **96**, 027203 (2006).

23. Florin Radu1, Alexei Nefedov, Johannes Grabis, Gregor Nowak, Andre Bergmann, Hartmut Zabel, J. Magn. Magn. Mater. **300**, 206 (2006).

24. Sebastian Brück, Gisela Schütz, Eberhard Goering, Xiaosong Ji, and Kannan M. Krishnan, Phys. Rev. Lett. **101**, 126402 (2008).

25. P. Miltényi, M. Gierlings, J. Keller, B. Beschoten, G. Güntherodt, U. Nowak, and K. D. Usade, Phys. Rev. Lett. **84**, 4224 (2000).

26. Jung-Il Hong, Titus Leo, David J. Smith, and Ami E. Berkowitz, Phys. Rev. Lett. **96**, 117204 (2006).

27. Marian Fecioru-Morariu, Syed Rizwan Ali, Cristian Papusoi, Martin Sperlich, and Gernot Güntherodt, Phys. Rev. Lett. **99**, 097206 (2007).

28. U. Nowak, K. D. Usadel, J. Keller, P. Miltényi, B. Beschoten, and G. Güntherodt, Phys. Rev. B **66**, 014430 (2002).

29. R. Morales, Zhi-Pan Li, J. Olamit, Kai Liu, J. M. Alameda, and Ivan K. Schuller, Phys. Rev. Lett. **102**, 097201 (2009).

30. A. Scholl, M. Liberati, E. Arenholz, H. Ohldag, and J. Stöhr, Phys. Rev. Lett. **92**, 247201 (2004).

31. A. Brambilla, P. Sessi, M. Cantoni, L. Duò, M. Finazzi and F. Ciccacci, Thin Solid Films **516**, 7519 (2008).

32. Gerrit van der Laan, Elke Arenholz, Rajesh V. Chopdekar and Yuri Suzuki, Phys. Rev. **B 77**, 064407 (2008).

33. Elke Arenholz, Gerrit van der Laan,, Rajesh V. Chopdekar, and Yuri Suzuki, Phys. Rev. Lett. **98**, 197201 (2007).

34. I. P. Krug, F. U. Hillebrecht, M. W. Haverkort, A. Tanaka, L. H. Tjeng, H. Gomonay, A. Fraile-Rodríguez, F. Nolting, S. Cramm, and C. M. Schneider, Phys. Rev. B **78**, 064427 (2008).